Journal of Power Sources 209 (2012) 204–208

Contents lists available at SciVerse ScienceDirect

Journal of Power Sources

journal homepage: www.elsevier.com/locate/jpowsour

Short communication

Synthesis of mesoporous Sn–Cu composite for lithium ion batteries

Jizhang Chen [a], Li Yang [a,*], Shaohua Fang [a], Shin-ichi Hirano [b]

[a] School of Chemistry and Chemical Engineering, Shanghai Jiaotong University, Shanghai 200240, China
[b] Hirano Institute for Materials Innovation, Shanghai Jiaotong University, Shanghai 200240, China

ARTICLE INFO

Article history:
Received 13 January 2012
Received in revised form 12 February 2012
Accepted 28 February 2012
Available online 7 March 2012

Keywords:
Tin
Copper
Mesoporous
Lithium ion batteries

ABSTRACT

Mesoporous Sn–Cu composite consisting of Cu_6Sn_5 (active), Cu_3Sn (inactive), and Sn is prepared by using silica SBA-15 as the hard template. As-prepared composite has a large BET surface area of 197.8 $m^2\,g^{-1}$ and a large pore volume of 0.517 $cm^3\,g^{-1}$. As the anode material for lithium ion batteries, no obvious capacity decay can be observed from 2nd to 20th cycles when the current density is 500 mA g^{-1}. It delivers much better cycling performance than bulk Sn–Cu composite without porous structure. The mesoporous structure can provide sufficient contact of the active material with the electrolyte, and can buffer volume changes of Sn in the electrochemical process. Charge transfer process is also found to be favored by using EIS measurements.

1. Introduction

The finite supply of petroleum and the request for low carbon economy have aroused substantial research in electric vehicles (EV) and hybrid electric vehicles (HEV). As the best choice as power source for EV and HEV, lithium ion batteries (LIBs) have attracted tremendous interest worldwide [1,2]. The future application of LIBs requires high safety, high energy density, and high power density. Metallic tin (Sn) can alloy with lithium as $Li_{4.4}Sn$, with a theoretical specific capacity of 991 mAh g^{-1} or 7313 mAh cm^{-3}, much larger than graphite (merely 372 mAh g^{-1} or 833 mAh cm^{-3}). Furthermore, the operating potential of Sn is slightly higher than graphite, contributing to higher safety [3]. Unfortunately, the alloy process of Sn is accompanied by great volume expansion, which would induce cracking of Sn and loss of conductivity at the electrode, causing the capacity to degrade very quickly [4]. To combat this problem, many tactics have been employed, including decreasing the size of the active material to nanoscale [5,6], embedding Sn-contained active materials in a carbon matrix [7–10], and alloying Sn with other metallic elements which are inactive to lithium (e.g., Cu [11–14], Co [15–17], Ni [18–20], Fe [21]). All these strategies are aimed at buffering volume changes of Sn and suppressing pulverization of the active material. Except for these strategies, porous structure (e.g., three-dimensional porous Sn thin film [11] and ordered mesoporous Sn–Cu composite [10]) is also effective in accommodating structural strain associated with volume change, and it can guarantee sufficient contact of the active material with the electrolyte, thus favoring charge transfer process and lowering polarization.

In this work, we report for the first time to our knowledge, mesoporous Sn–Cu composite for LIBs. It is prepared by using two-dimensional hexagonal silica SBA-15 (space group *P6mm*) as the template. Mesoporous materials such as $LiCoO_2$ [22], MoO_2 [23], and TiO_2 [24], prepared by such hard templating method have already been reported to be advanced electrode materials with excellent cycling performances. As for Sn, which has a rather low melting point of 232 °C and active to both acid and alkali, it is very difficult to obtain mesoporous structure. Herein, we use Cu as the skeleton to restrict the aggregation of Sn, and mesoporous Sn–Cu composite is successfully fabricated. As-prepared composite are composed of Cu_6Sn_5, Cu_3Sn and Sn, with a large surface area of 197.8 $m^2\,g^{-1}$ and a large pore volume of 0.517 $cm^3\,g^{-1}$. As the anode material for LIBs, it delivers much better cycling performance than bulk Sn–Cu composite without porous structure.

2. Experimental

2.1. Sample preparation and characterization

All chemicals were used as received. Mesoporous silica SBA-15 was prepared according to literature methods [25]. 0.15 g SBA-15 was dispersed in 5 mL deionized water, then 1 mmol $SnCl_4{\cdot}5H_2O$ and 0.6 mmol $Cu(CH_3COO)_2{\cdot}H_2O$ were added. After stirred for 1 h, the suspension was poured into a dish and kept at 60 °C under vacuum for 10 h. The powder was scraped from the dish, and heated at 320 °C in a reducing atmosphere (5% H_2 in Ar) for 4 h. As-collected

* Corresponding author. Tel.: +86 21 54748917; fax: +86 21 54741297.
E-mail address: liyangce@sjtu.edu.cn (L. Yang).

0378-7753/$ – see front matter © 2012 Elsevier B.V. All rights reserved.
doi:10.1016/j.jpowsour.2012.02.111

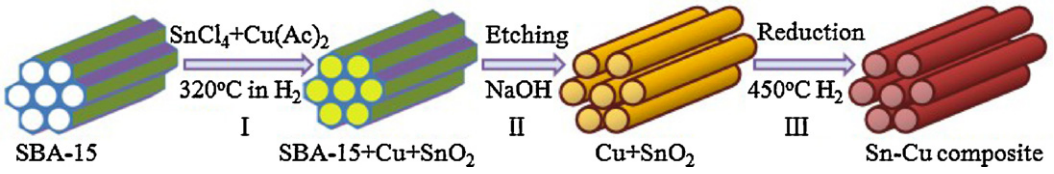

Fig. 1. Schematic illustration of the fabrication process.

powder was dispersed in 100 mL 0.5 M NaOH aqueous solution and stirred at 50 °C for 1 h to etch SBA-15. After centrifugation, washed with deionized water thoroughly and then dried at 60 °C under vacuum, the powder was heated at 450 °C in a reducing atmosphere (5% H_2 in Ar) for 4 h to obtain the Sn–Cu composite. The composition and crystal structure of the products were characterized by X-ray diffraction measurement (XRD, Rigaku, D/max-Rbusing Cu Kα radiation). The morphology and microstructure were obtained using field emitting scanning electron microscopy (FE-SEM, JEOL JSM-7401F) and transmission electron microscopy (TEM, JEOL JEM-2010). The N_2 adsorption/desorption tests were carried out by Micromeritics ASAP 2010 instrument.

2.2. Electrode preparation and electrochemical characterization

Electrochemical measurements were performed using 2016-type coin cells assembled in an argon-filled glove box (German, M. Braun Co., [O_2] < 1 ppm, [H_2O] < 1 ppm). For preparing working electrodes, a mixture of the active material, acetylene black, and polyvinylidene fluoride (PVDF) binder at a weight ratio of 80:10:10 was pasted on pure copper foil. After vacuum drying, this foil was cut into rounded electrodes with a diameter of 14 mm (ca. 2 mg Sn–Cu composite on each electrode). Pure lithium foil was used as the counter electrode. A glass fiber (GF/A) from Whatman was used as the separator. The electrolyte consisted of a solution of 1 M $LiPF_6$ in ethylene carbonate and dimethyl carbonate (EC + DMC) (1:1 in volume). The cells were cycled under 500 mA g^{-1} between cutoff voltages of 2 and 0.01 V on a CT2001A cell test instrument (LAND Electronic Co.) at room temperature. Cyclic voltammetry (CV) and electrochemical impedance spectroscopy (EIS) were implemented on a CHI660D electrochemical workstation.

3. Results and discussion

Fig. 1 describes the fabrication process, and Fig. 2 shows wide-angle and small-angle XRD patterns of the products before and after step III. In the step I, Sn and Cu precursors were casted into SBA-15 and then heat treated in a reducing atmosphere (5% H_2 in Ar). Then, after etching SBA-15 in NaOH aqueous solution, we obtained Cu–SnO_2 composite, which possessed reverse hexagonal structure of SBA-15, with [1 0 0] peak observed in Fig. 2b. In the step III, SnO_2 was in situ reduced to Sn. Due to its low melting point (232 °C), Sn would liquefy and aggregate in the reduction process. In our strategy, Cu could act as the skeleton to alloy with Sn and restrict the aggregation. After step III, Sn–Cu composite consisting of three phases (Cu_6Sn_5, Cu_3Sn, Sn) was obtained (see Fig. 2a). The mass fractions of Cu_6Sn_5, Cu_3Sn and Sn are 53.81%, 31.67%, and 14.52%, respectively, calculated form RIR method of XRD analysis. Seen in Fig. 2b, the [1 0 0] peak disappeared after reduction at 450 °C. This might be caused by the existence of Sn, liquefying and dispersing nonuniformly in the mesopores, resulting in the nonuniformity of the mesoporous structure (i.e., the sizes of mesopores and walls are not uniform). The existence of Cu_3Sn is inevitable in this reaction system, due to the low melting point of tin. Unlike Cu_6Sn_5 and Sn, Cu_3Sn is inactive to lithium [26,27], consequently it can buffer volume changes of the composite, beneficial to the cycling performance.

As shown in Fig. 3, N_2 adsorption/desorption isotherms of as-prepared Sn–Cu composite displays type IV isotherms with a representative H_1-type hysteresis loop, indicating the mesoporosity, which can also be confirmed by Barrett–Joyner–Halanda (BJH) desorption pore-size distributions (inset). The total pore volume is 0.517 cm^3 g^{-1} and the specific surface area calculated from Brunauer–Emmett–Teller (BET) method is as large as 197.8 m^2 g^{-1}.

Further structural characterization of our products was implemented by using SEM and TEM technologies. Fig. 4a reveals a panoramic SEM micrograph of as-prepared Sn–Cu composite, whose shape is uniform and similar to the cylinder. From Fig. 4b, rough surface and porous structure can be clearly seen. Fig. 4c displays TEM image of Sn–Cu composite, indicative of mesoporous structure. TEM images viewed from [1 0 0] and [0 0 1] directions are presented in Fig. 4d.

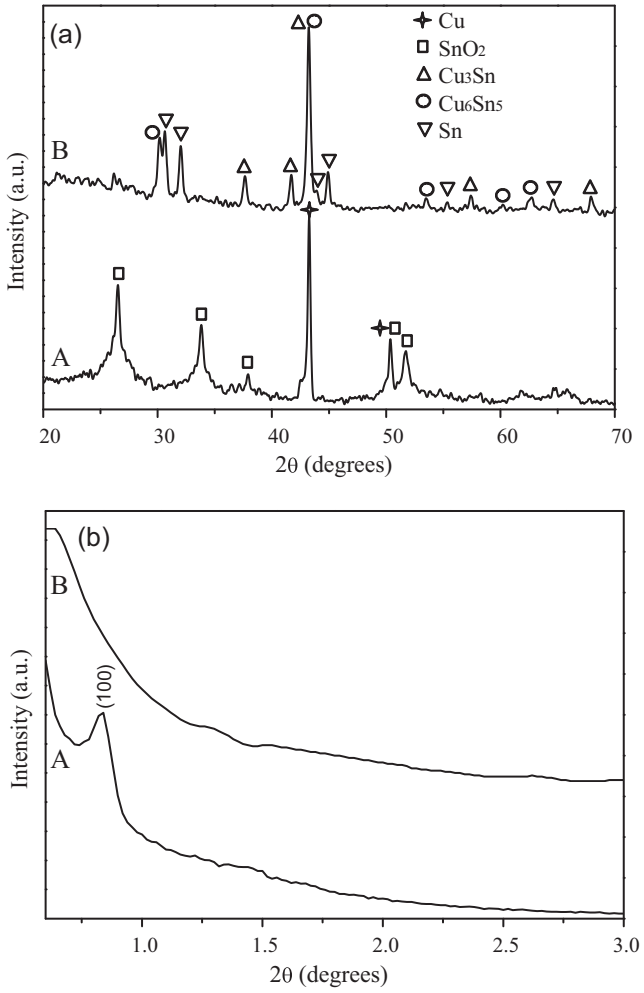

Fig. 2. (a)Wide-angle and (b) small-angle XRD patterns of the products (A) before and (B) after step III.

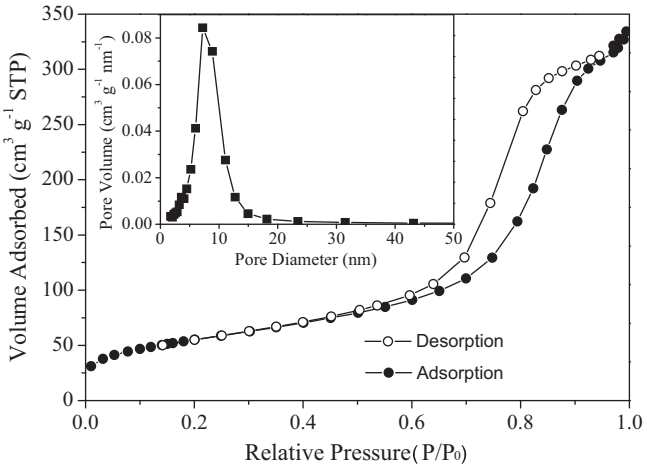

Fig. 3. N_2 adsorption and desorption isotherms of mesoporous Sn–Cu composite. The inset shows corresponding BJH pore-size distributions.

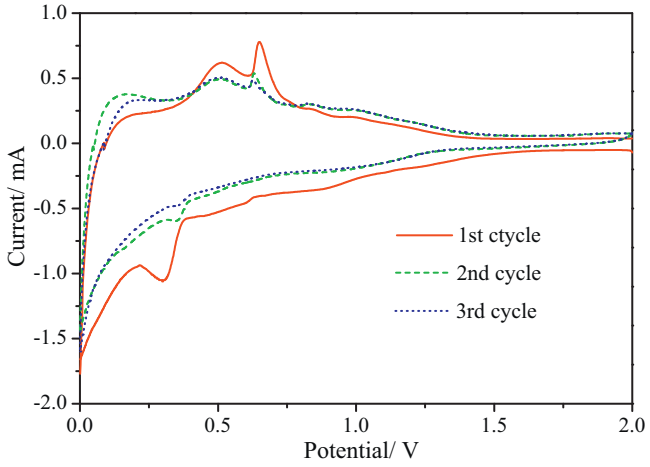

Fig. 5. Cyclic voltammograms of mesoporous Sn–Cu composite at a scan rate of 0.5 mV s^{-1} between 2.0 and 0 V.

Fig. 5 shows CV curves of as-prepared mesoporous Sn–Cu composite cycled in 1 M $LiPF_6$ EC/DMC electrolyte solution at scan rates of 0.5 mV s^{-1}. In the first cycle, the cathodic peaks above 0.4 V could be mainly ascribed to Sn alloying with Li and the decomposition of the electrolyte. The well-resolved peak at ca. 0.3 V could be assigned to the formation of Li_xSn from Cu_6Sn_5, which became very weak in the second cycle and nearly disappeared in the third cycle. The reduction process below 0.3 V is the stepwise formation process of $Li_{4.4}Sn$. In the anodic curve, multiple humps located at around 0.11, 0.51, and 0.65 V are observed, corresponding to the de-alloying process. In addition, the nearly overlapped second and third cycles are indicative of good capacity retention after the first cycle.

The electrochemical property of mesoporous Sn–Cu composite was studied by galvanostatic method using Sn–Cu/Li half cells. For comparison, bulk Sn–Cu composite prepared without SBA-15 template was also investigated. Given that the theoretical specific capacities of Sn and Cu_6Sn_5 are 991 and 603 mAh g^{-1}, the theoretical specific capacity of as-prepared Sn–Cu composite is 468 mAh g^{-1}. Fig. 6a displays cycling performances of mesoporous and bulk Sn–Cu at 500 mA g^{-1} (ca. 1.07 C). In the 1st cycle, mesoporous Sn–Cu delivered a discharge capacity of 530.4 mAh g^{-1}, which declined to 443.2 mAh g^{-1} in the 2nd cycle, and 445 mAh g^{-1} in the 3rd cycle. The capacity beyond theoretical value in the 1st cycle is due to the decomposition of the electrolyte, and 94.7% and 95.1% of theoretical capacity are realized in 2nd and 3rd cycles,

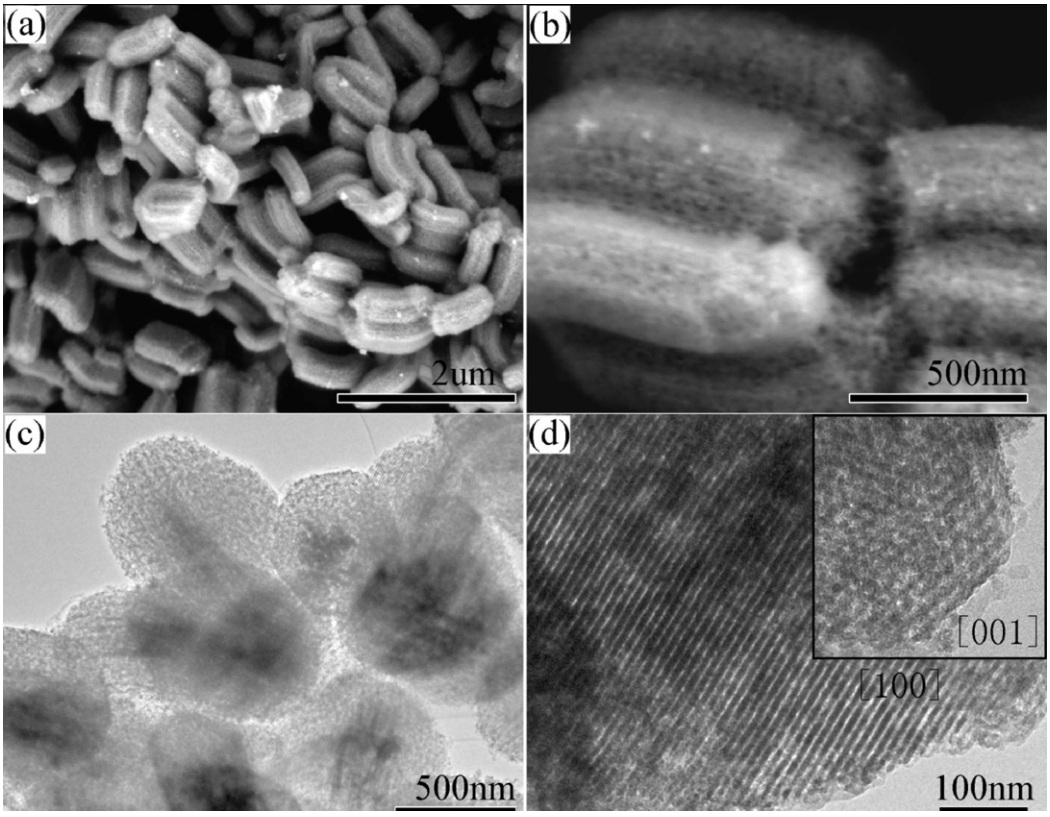

Fig. 4. (a and b) SEM and (c and d) TEM images of mesoporous Sn–Cu composite with different magnification.

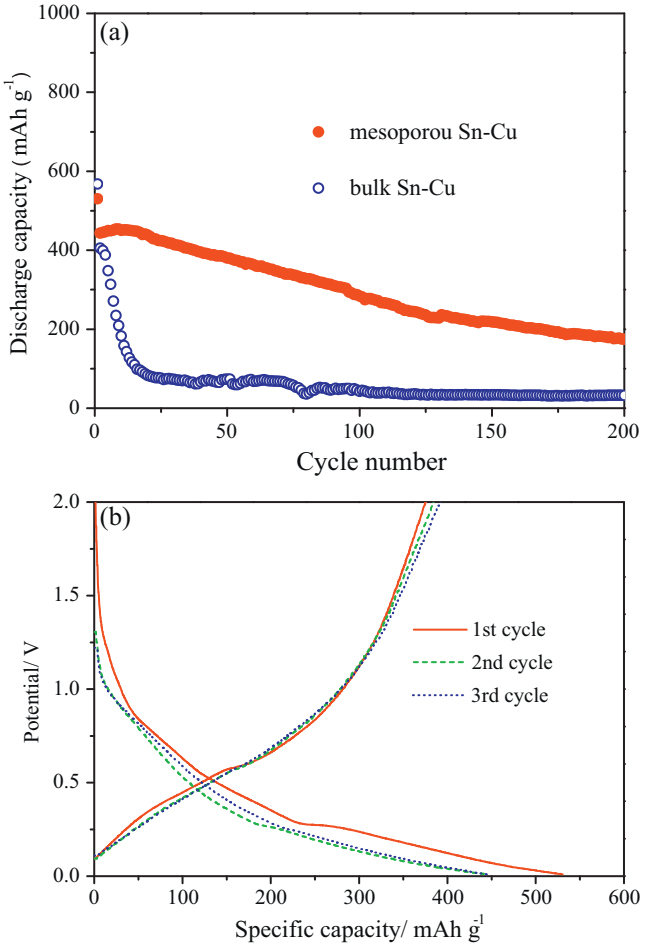

Fig. 6. (a) Cycle performances of mesoporous Sn–Cu and bulk Sn–Cu at 500 mA g^{-1} and (b) initial three discharge/charge curves of mesoporous Sn–Cu.

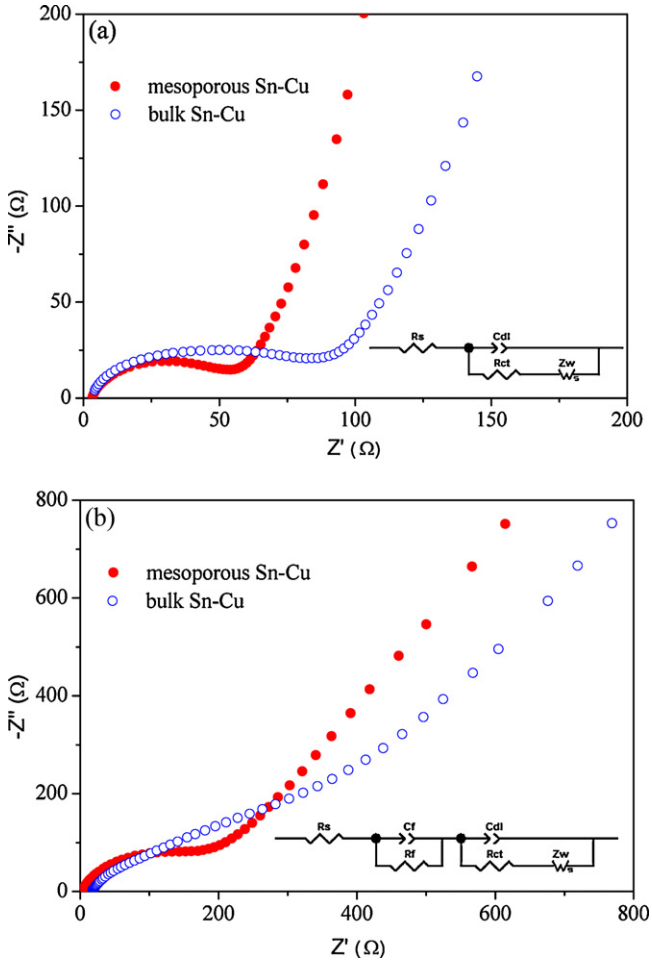

Fig. 7. Nyquist plots of mesoporous Sn–Cu and bulk Sn–Cu (a) before and (b) after 200 galvanostatic cycles.

respectively. After that, no obvious capacity decay was observed in initial 20 cycles at such a large current density of 500 mA g^{-1}. In the repeated discharge/charge process, Sn would expand and contract, as a result, part of Sn began pulverizing and cracking, inducing capacity fading after 20 cycles. The capacity slowly decreased to 174.5 mAh g^{-1} at 200th cycle. Although the capacity retention is merely 32.9% after 200 cycles, the cycling stability of mesoporous Sn–Cu is no worse than Refs. [11–14] (Sn–Cu). As for bulk Sn–Cu, the capacity dropped very rapidly. The improved cycling performance of our sample is rooted in 'its unique mesoporous structure. First, the hierarchical mesoporosity makes facile diffusion of the liquid electrolyte into the interior of the active material, and hence provides fast conductive Li^+ transport channels. The mesoporous channels could also buffer volume changes of Sn in the alloying/de-alloying process, thus enhancing the structural stability. Second, the large surface area of the active material could ensure a large electrode/electrolyte contact area, and the thin walls of mesoporous Sn–Cu could significantly reduce the solid diffusion of Li^+. Finally, the micrometer-sized whole block particle could provide a thermodynamically stable system. The initial three discharge/charge curves are presented in Fig. 6b, showing typical sloping voltage profile associated with lithium alloying–dealloying with nanosized Sn. As in the 1st cycle, a short discharge plateaus at about 0.3 V was observed, in good agreement with CV results. The coulombic efficiencies of the initial three cycles are 70.8%, 86.8%, and 88.2%, respectively.

Electrochemical impedance spectroscopy (EIS) was implemented to investigate mesoporous and bulk Sn–Cu composites before and after 200 cycles in the frequency range from 1×10^5 Hz to 1 Hz with perturbation amplitude of 5 mV and typical Nyquist plots are provided in Fig. 7. The high frequency intercept of the semicircle is generally considered as the bulk resistance of electrolyte (R_s). The depressed semicircles at high/medium frequency are reflective of SEI impedance R_f and charge transfer impedance R_{ct}, and the inclined lines at low frequency correspond to lithium diffusion within the active material. The equivalent circuits in the inset of Fig. 7 were used to fit EIS spectra, and the fitting results are summarized in Table 1. R_s of mesoporous and bulk Sn–Cu nearly equaled (ca. 3.1 Ω) before cycles, and turned out to 3.5 and 16 Ω after cycles. Before cycles, R_{ct} of mesoporous and bulk Sn–Cu were 54 and 83 Ω, indicating that mesoporous Sn–Cu has a lower charge transfer resistance, favoring for lithium diffusion. After 200 cycles, R_{ct} increased to 174 Ω for mesoporous Sn–Cu and became very large (cannot be fitted) for bulk Sn–Cu, and this could explain why mesoporous Sn–Cu has a much better cycling performance. In fact,

Table 1
The fitting results of R_s, R_f, and R_{ct} (Ω) of mesoporous Sn–Cu and bulk Sn–Cu from EIS measurements.

	Mesoporous Sn–Cu		Bulk Sn–Cu	
	Before cycles	After 200 cycles	Before cycles	After 200 cycles
R_s	3.125	3.503	3.052	16.21
R_f	Null	12.54	Null	Null
R_{ct}	53.52	174.5	82.6	Null

severe pulverization has occurred for bulk Sn–Cu, while it is eased for mesoporous Sn–Cu.

4. Conclusions

In summary, we have obtained mesoporous Sn–Cu composite by using a nanocasting method. As-prepared composite is comprised of Cu_6Sn_5, Cu_3Sn, and Sn. Among them, Cu_3Sn can help buffer volume changes of Sn and Cu_6Sn_5 in the alloying process. The composite has highly mesoporous structure and a large surface area of 197.8 $m^2\ g^{-1}$, contributing to sufficient contact of the active material with the electrolyte, facile lithium diffusion, and accommodation of the structural strain. Compared with bulk Sn–Cu composite without porous structure, our sample gives much better cycling performance. EIS measurements demonstrate that charge transfer process is significantly enhanced and pulverization is eased by employing mesoporous structure.

Acknowledgements

This work was performed with the financial support from the National Natural Science Foundation of China (Grants No. 21103108 and 21173148) and Shanghai Jiao Tong University Innovation Fund for Postgraduates. The authors thank the Research Center of Analysis and Measurement of Shanghai Jiao Tong University for the help of characterization.

References

[1] M.R. Palacín, Chem. Soc. Rev. 38 (2009) 2565.
[2] B. Scrosati, J. Garche, J. Power Sources 195 (2010) 2419.
[3] M. Winter, J.O. Besenhard, M.E. Spahr, P. Novák, Adv. Mater. 10 (1998) 725.
[4] J.O. Besenhard, J. Yang, M. Winter, J. Power Sources 68 (1997) 87.
[5] Y.H. Yu, Q. Yang, D.H. Teng, X.P. Yang, S.K. Ryu, Electrochem. Commun. 12 (2010) 1187.
[6] R. Yang, J. Huang, W. Zhao, W.Z. Lai, X.Z. Zhang, J. Zheng, X.G. Li, J. Power Sources 195 (2010) 6811.
[7] L. Zou, L. Gan, F.Y. Kang, M.X. Wang, W.C. Shen, Z.H. Huang, J. Power Sources 195 (2010) 1216.
[8] S.Z. Liang, X.F. Zhu, P.C. Lian, W.S. Yang, H.H. Wang, J. Solid State Chem. 184 (2011) 1400.
[9] P. Wu, N. Du, J. Liu, H. Zhang, J.X. Yu, D.R. Yang, Mater. Res. Bull. 46 (2011) 2278.
[10] J.Z. Chen, L. Yang, S.H. Fang, S. Hirano, Electrochem. Commun. 13 (2011) 848.
[11] Q.Y. Li, S.J. Hu, H.Q. Wang, F.P. Wang, X.X. Zhong, X.Y. Wang, Electrochim. Acta 54 (2009) 5884.
[12] J.W. Park, J.Y. Eom, H.S. Kwon, Electrochim. Acta 55 (2010) 1825.
[13] X.Y. Zhao, Z.H. Xia, D.G. Xia, Electrochim. Acta 55 (2010) 6004.
[14] S.C. Zhang, Y.L. Xing, T. Jiang, Z.J. Du, F. Li, L. He, W.B. Liu, J. Power Sources 196 (2011) 6915.
[15] C.G. Yang, D.W. Zhang, Y.B. Zhao, Y.H. Lu, L. Wang, J.B. Goodenough, J. Power Sources 196 (2011) 10673.
[16] K. Ui, S. Kikuchi, Y. Jimba, N. Kumagai, J. Power Sources 196 (2011) 3916.
[17] L.J. Xue, Y.F. Xu, L. Huang, F.S. Ke, Y. He, Y.X. Wang, G.Z. Wei, J.T. Li, S.G. Sun, Electrochim. Acta 56 (2011) 5979.
[18] S.W. Woo, N. Okada, M. Kotobuki, K. Sasajima, H. Munakata, K. Kajihara, K. Kanamura, Electrochim. Acta 55 (2010) 8030.
[19] H.R. Jung, E.J. Kim, Y.J. Park, H.C. Shin, J. Power Sources 196 (2011) 5122.
[20] J. Hassoun, G.A. Elia, S. Panero, B. Scrosati, J. Power Sources 196 (2011) 7767.
[21] R.G. Zhang, S. Upreti, M.S. Whittingham, J. Electrochem. Soc. 158 (2011) A1498.
[22] F. Jiao, K.M. Shaju, P.G. Bruce, Angew. Chem. Int. Ed. 44 (2005) 6550.
[23] Y.F. Shi, B.K. Guo, S.A. Corr, Q.H. Shi, Y.S. Hu, K.R. Heier, L.Q. Chen, R. Seshadri, G.D. Stucky, Nano Lett. 9 (2009) 4215.
[24] W.B. Yue, C. Randorn, P.S. Attidekou, Z.X. Su, J.T.S. Irvine, W.Z. Zhou, Adv. Funct. Mater. 19 (2009) 2826.
[25] D.Y. Zhao, J.L. Feng, Q.S. Huo, N. Melosh, G.H. Fredrickson, B.F. Chmelka, G.D. Stucky, Science 279 (1998) 548.
[26] N. Tamura, R. Ohshita, M. Fujimoto, M. Kamino, S. Fujitani, J. Electrochem. Soc. 150 (2003) A679.
[27] J.Y. Kwon, J.H. Ryu, Y.S. Jung, S.M. Oh, J. Alloys Compd. 509 (2011) 7595.